JOURNAL OF MOLECULAR SPECTROSCOPY **192,** 162–168 (1998)
ARTICLE NO. MS987684

Cavity-Ring-Down Spectroscopy on the $b^1\Sigma_g^+$–$X^3\Sigma_g^-$ (1,0) Band of Oxygen Isotopomers

H. Naus, S. J. van der Wiel, and W. Ubachs

Laser Centre, Department of Physics and Astronomy, Vrije Universiteit, De Boelelaan 1081, 1081 HV Amsterdam, The Netherlands

Received March 31, 1998; in revised form July 14, 1998

The $b^1\Sigma_g^+$–$X^3\Sigma_g^-$ (1,0) band of $^{16}O^{17}O$, $^{16}O^{18}O$, $^{18}O_2$, $^{17}O^{18}O$, and $^{17}O_2$ isotopomers was investigated employing the technique of cavity-ring-down spectroscopy. More than 400 transition frequencies of magnetic dipole lines were determined with a typical uncertainty of 0.01 cm^{-1}. This work results in new or improved accurate molecular constants for the excited $b^1\Sigma_g^+$, $v = 1$ state of all isotopomers and for the $X^3\Sigma_g^-$, $v = 0$ ground state of $^{17}O_2$.

1. INTRODUCTION

The oxygen *A* and *B* bands, corresponding to the (0,0) and (1,0) bands of the $b^1\Sigma_g^+$–$X^3\Sigma_g^-$ system are prominent features in the absorption spectrum of the terrestrial atmosphere. Nevertheless these bands are very weak due to the strongly forbidden character of gerade-gerade and Σ^+–Σ^- transitions, and they can only be observed via a magnetic dipole transition moment. The atmospheric *B* band, the subject of the present investigation, has an experimentally determined radiative rate $A(1,0)$ ranging from 0.0069 s^{-1} (*1*) to 0.00724 s^{-1} (*2, 3*). Recent *ab initio* calculations yield a rate of 0.00954 s^{-1} (*4*). These values correspond to an oscillator strength of $f_{10} = 1.6 \times 10^{-11}$. Hence the oxygen *B* band is 10 orders of magnitude weaker than ordinary electric dipole-allowed transitions. Spectroscopically the *b*–*X* (1,0) band was studied by Babcock and Herzberg (*5*). Their data were reanalyzed by computer fitting procedures to yield accurate and consistent molecular constants for ground and excited electronic states (*6*). Later the (1,0) band was reinvestigated by Fourier-transform methods resulting in accurate constants and pressure shift parameters (*7, 8*). These latter studies concentrated on the $^{16}O_2$ molecule, while Babcock and Herzberg also observed the $^{16}O^{18}O$ and $^{16}O^{17}O$ isotopomers.

The technique of cavity-ring-down (CRD) laser spectroscopy, invented by O'Keefe and Deacon (*9*), has in recent years been developed into a tool for quantitative measurement of very weak absorptions (*10–12*). It has been applied to study some weak systems in oxygen, the *A* band in the near infrared (*13, 14*), as well as the Herzberg systems in the ultraviolet (*15*). In this work the CRD technique is employed for a spectroscopic study of the *B* band for all oxygen isotopomers other than $^{16}O_2$ resulting in new or improved molecular constants for the $b^1\Sigma_g^+$, $v = 1$ state.

2. EXPERIMENTAL PROCEDURES

The experimental setup, schematically shown in Fig. 1, is similar to the setup previously used for a study of the *A* band (*14*) with the exception of the wavelength calibration part. Tunable radiation near 688 nm, in pulses of 5-ns duration and a repetition rate of 10 Hz, is obtained from a Nd:YAG pumped pulsed dye laser running on Pyridine-1 dye. For the principles of converting the ring-down transients into an absorption spectrum we refer to Refs. (*9–13*). With highly reflecting mirrors ($R \approx 99.998\%$, Research Electro Optics) transients with decay times of 50–60 μs were established, corresponding to an effective absorption path of 50 km (3τ). The CRD-spectra of $^{16}O^{18}O$ and $^{17}O^{18}O$ isotopomers were recorded in static gas of ≈30 Torr from a ^{18}O-enriched sample (Euristop, 95% $^{18}O_2$), in which the signals on $^{18}O_2$ lines were saturated (see Fig. 2), i.e., deviate from the linear approximation of Beer's law. The $^{18}O_2$-linepositions were

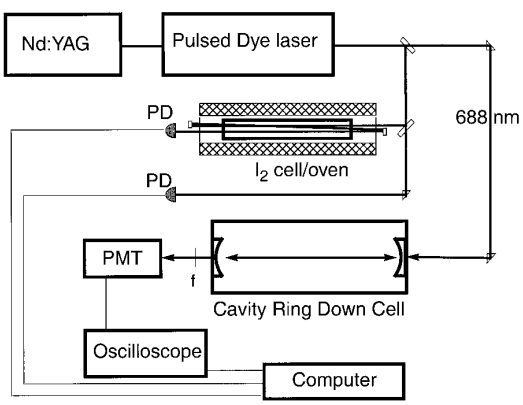

FIG. 1. Experimental setup. PD, photodiodes; PMT, photomultiplier; f, optical bandpass filter.

0022-2852/98 $25.00

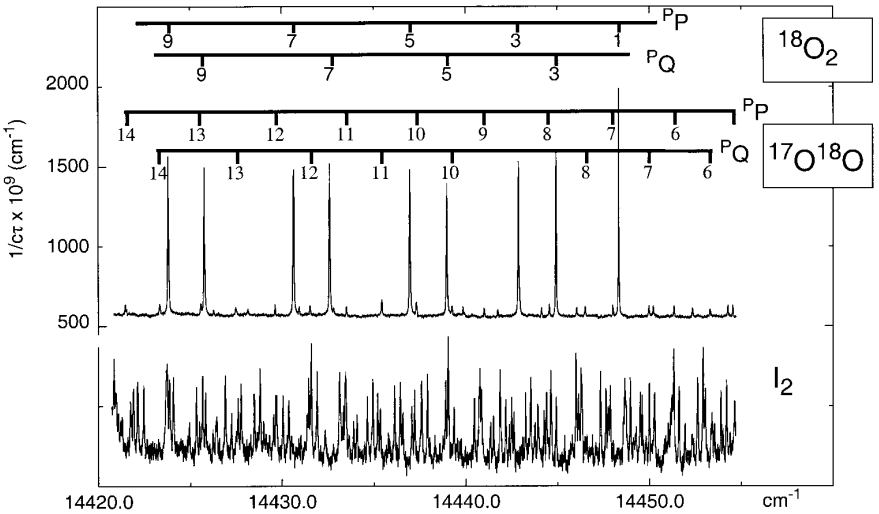

FIG. 2. CRD spectrum from a (95%) $^{18}O_2$-enriched sample at 31.6 Torr (top) and a simultaneously recorded I_2-absorption spectrum after intensity normalization (bottom). $^{18}O_2$ lines, as indicated, are saturated. This spectrum was used to determine linepositions of $^{17}O^{18}O$. Some weak $^{16}O^{18}O$ lines are visible (not marked).

measured from a sample at 1 Torr. A ^{17}O-enriched sample (Campro Scientific, 50% ^{17}O atom) was used to record spectra of $^{17}O_2$ and $^{16}O^{17}O$ isotopomers, which appeared to have equal intensity.

The O_2 spectra are somewhat manipulated before being used for analysis. As often in recorded CRD spectra, an oscillation occurs on the absorption baseline, in our case having a period of 0.9 cm^{-1}. The exact origin of this phenomenon is not known, but from the evidences gathered we ascribe it to beating of high-order modes that undergo different decay times in the high-Q cavity. Via a computerized method the baseline oscillation was subtracted from the absorption spectrum. At O_2 pressures below 30 Torr the pressure-induced shift is 0.001–0.002 cm^{-1} (*7*), so negligibly small in the present experiment. Doppler broadening, 0.03 cm^{-1} for the b-X(1,0) band at room temperature, contributes somewhat to the observed linewidth, which is dominated by the laser bandwidth of 0.06 cm^{-1}.

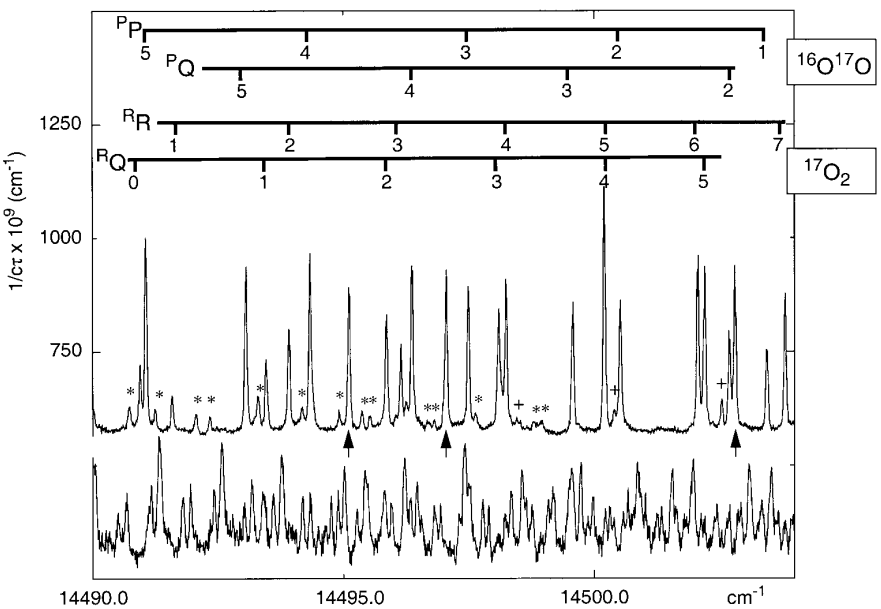

FIG. 3. CRD spectrum from a (50% atom) ^{17}O-enriched sample at 16.5 Torr (top) and a simultaneously recorded I_2-absorption spectrum after intensity normalization (bottom). $^{16}O^{17}O$ and $^{17}O_2$ lines as indicated. Resonances marked with * are $^{17}O^{18}O$. Additional resonances due to $^{16}O^{18}O$ are also visible (marked with +), while three intense resonances of $^{16}O_2$ are marked with an arrow.

TABLE 1
$^{16}O^{17}O$

	$P_{Q(N)}$		$P_{P(N)}$		$R_{R(N)}$		$R_{Q(N)}$	
N	Obs.	o.-c.	Obs.	o.-c.	Obs.	o.-c.	Obs.	o.-c.
1			14503.454	-.008	14511.453	-.005	14513.337	-.006
2	14502.707	-.005	14500.526	-.020	14513.873	.000	14515.793	-.007
3	14499.575	-.007	14497.495	-.011	14516.166	.003	14518.111	-.005
4	14496.369	-.006	14494.339	-.001	14518.321	-.005	14520.309	.010
5	14493.057	-.001	14491.058	.008	14520.362	-.002	14522.360	.007
6	14489.633	.009	14487.656	.021	14522.275	-.001	14524.281	.002
7	14486.087	.019	14484.103	.007	14524.057	-.004	14526.080	.002
8	14482.383	-.007	14480.426	-.006	14525.707	-.014	14527.746	-.003
9	14478.589	.000	14476.646	.003	14527.238	-.015	14529.292	.000
10	14474.674	.010	14472.745	.015	14528.653	-.006	14530.709	.000
11	14470.623	.008	14468.690	-.003	14529.948	.011	14531.994	-.003
12	14466.444	.002	14464.537	.006	14531.097	.009	14533.171	.013
13	14462.148	.002	14460.248	.004	14532.112	.000	14534.193	.001
14	14457.733	.009	14455.843	.011	14533.023	.015	14535.095	-.002
15	14453.178	-.001	14451.309	.013	14533.774	-.001	14535.861	-.013
16	14448.506	-.003	14446.619	-.017	14534.420	.006	14536.521	-.001
17	14443.717	.003	14441.854	.004	14534.930	.006	14537.032	-.009
18	14438.790	-.005	14436.932	-.008	14535.286	-.019	14537.427	-.004
19	14433.764	.013	14431.917	.012	14535.540	-.017	14537.691	-.001
20	14428.586	.004	14426.737	-.008	14535.672	-.007	14537.816*	-.007
21	14423.274	-.014	14421.445	-.015			14537.816*	-.007
22	14417.878	.010	14416.061	.012				
23	14412.319	-.005	14410.498	-.015				
24	14406.648	-.006	14404.848	-.004				
25	14400.877	.019	14399.083	.018				
26	14394.944	.007	14393.154	.002				
27	14388.880	-.009	14387.104	-.009				
28	14382.770*	.054	14380.956	.008				
29	14376.409	-.007	14374.663	.006				

* blended lines

For the purpose of wavelength calibration an absorption spectrum of molecular iodine was recorded simultaneously with the CRD spectrum of oxygen. Since in the wavelength range near 688 nm I_2 has strong transitions in the *B-X* system for (v', v' = 6) bands, the I_2-sample was heated in an oven to 430 K, to reach sufficient population of v'' = 6 levels. From the weight of solid iodine evaporated in the cell an operation pressure of 60 Torr I_2 gas is estimated at which the absorption measurements are performed. At these pressures collisional broadening of I_2 lines does occur, but not in the amount to affect the width of the observed resonances (0.07 cm^{-1}). Pressure-induced shifts at 60 Torr in I_2 are on the order of 0.002 cm^{-1}. Three passes through the heated I_2 cell creates a total absorption length of 1.4 m. The signal-to-noise ratio of the thus observed I_2 absorption spectrum is improved by normalizing to the laser power, measured for each pulse on a separate photodiode.

With computerized fitting the peak positions were determined in the I_2 spectra. Subsequently, after identification of the I_2 lines, the frequencies of the I_2 atlas (*16*) were used to create a linearized frequency scale, which, in turn, was employed to calibrate the frequencies of the O_2 resonances. For the intense lines this produces results in an uncertainty of 0.01 cm^{-1}. In the experimental procedures wavelength steps of 0.01 cm^{-1} were taken. So 15 data points contribute to the line profile of 0.07 cm^{-1} width (FWHM).

In principle the CRD spectra can provide information on the absolute absorption strengths of the resonance lines. In our case such information could be derived from the calibrated vertical scales in Figs. 2 and 3. However, if CRD transients are induced by a light source, which is broader than the Doppler- and collisionally broadened spectral lines, intricate corrections have to be implemented to deduce reliable linestrengths (*11, 13*), and this was not pursued in the present study.

TABLE 2
$^{16}O^{18}O$

	$P_{Q(N)}$		$P_{P(N)}$		$R_{R(N)}$		$R_{Q(N)}$	
N	Obs.	o.-c.	Obs.	o.-c.	Obs.	o.-c.	Obs.	o.-c.
0							14493.211	.000
1			14486.104	.005	14493.857	-.025	14495.758	-.016
2	14485.410	-.004	14483.263	.001	14496.241	.007	14498.149	-.016
3	14482.376	.002			14498.453	-.011	14500.385	-.036
4			14477.233	.007	14500.535	-.038	14502.518	-.030
5	14476.042	.011	14474.026	.000	14502.518*	-.042	14504.543	-.008
6			14470.704	-.002	14504.411	-.013	14506.429	.000
7			14467.267	.002	14506.166	-.001	14508.195	.011
8	14465.670	.009	14463.716	.013	14507.794	.007	14509.833	.018
9	14461.976	.010	14460.018	-.003	14509.294	.010	14511.336	.013
10	14458.156	.004	14456.234	.016	14510.660	.001	14512.711	.003
11	14454.238	.020	14452.290	-.005	14511.902	-.008	14513.958	-.011
12	14450.152	-.011			14513.040	.001	14515.094	-.013
13	14445.982	-.006	14444.082	-.003	14514.031	-.012	14516.117	-.004
14	14441.690	-.003	14439.799	.000	14514.916	-.008	14516.996	-.015
15	14437.267	-.010	14435.394	.001	14515.661	-.019	14517.786	.010
16	14432.759	.018	14430.877	.012	14516.310	-.002	14518.426	.008
17	14428.093	.010	14426.217	.000	14516.814	-.006	14518.940	.006
18	14423.299	-.006			14517.193	-.009	14519.352*	.027
19					14517.458*	-.001	14519.625*	.035
20	14413.369	-.016	14411.542	-.003	14517.595*	.005	14519.758*	.028
21	14408.246	.003			14517.595*	.000	14519.758*	-.006

* blended lines

3. RESULTS AND ANALYSIS

In Figs. 2 and 3 simultaneous recordings are shown of CRD spectra of O_2, for ^{18}O- and ^{17}O-enriched samples, respectively, and I_2-calibration spectra. Via the computerized calibration and interpolation procedure, described above, frequency positions of all isotopomer lines except $^{16}O_2$ were determined. The transition frequencies, presented in Tables 1–5 for the various isotopomers, were included on the input deck of a least squares fitting routine for each isotopomer, in which the excited state is represented by

$$E(N) = \nu_{10} + BN(N + 1) - DN^2(N + 1)^2,$$

while the $X^3\Sigma_g^-$, $v = 0$ ground state energies were represented by an effective Hamiltonian as given by Rouillé *et al.* (*17*). Except for $^{17}O_2$ the molecular constants for the ground state, rotational as well as spin-coupling constants, were kept fixed at the accurate values from far-infrared and microwave spectroscopy from Steinbach and Gordy (*18*) and Cazolli *et al.* (*19*). In our previous paper (*14*) a detailed listing of all relevant ground state constants was given.

In the weighted least squares fits the data were included with uncertainty of 0.01 cm^{-1} for the intense lines and 0.02 or 0.03 cm^{-1} for the weaker or partially overlapped lines. In that case the resulting χ^2 equals the number of data points, demonstrating that 0.01 cm^{-1} indeed represents the experimental uncertainty of the spectroscopic method. For each resonance line the deviation between measured transition frequency and calculated value is given in Tables 1–5. Molecular constants, resulting from the fitting procedures, for the $b^1\Sigma_g^+$, $v = 1$ excited state are presented in Table 6, with the errors representing one standard deviation. For comparison the most recent values for $^{16}O_2$ (*8*) are included in Table 6. The listed value of the band origin ν_{10} is dependent on the definition of the zero energy level. Usually the lowest energy state is chosen at zero energy, but in the case of $^{16}O_2$ and $^{18}O_2$ the $N = 0$, $J = 1$ level does not exist for symmetry reasons. Here we define zero at the energy given by the Rouillé Hamiltonian without spin and rotation, i.e., not at a specific level. With this definition the level $N = 0$, $J = 1$ is about 0.45 cm^{-1} below zero, slightly dependent on isotopomer. For clarity the values for the offset between $N = 0$, $J = 1$ levels and the trace of the Hamiltonian are given for each isotopomer in Table 6.

For the $X^3\Sigma_g^-$, $v = 0$ ground state of $^{17}O_2$ no accurate molecular constants are available, except from our previous study on the electronic *A* band (*14*). In a combined fit

TABLE 3
$^{17}O^{18}O$

	$P_{Q(N)}$		$P_{P(N)}$		$R_{R(N)}$		$R_{Q(N)}$	
N	Obs.	o.-c.	Obs.	o.-c.	Obs.	o.-c.	Obs.	o.-c.
1			14466.203	.019			14475.620	-.007
2	14465.588	.015	14463.422	-.015				
3	14462.633	.000	14460.567	-.006				
4	14459.629	.013					14482.194	.000
5	14456.496	.001	14454.512	.018	14482.141	-.003	14484.133	-.004
6	14453.272	.008	14451.275	-.006	14483.952	-.003	14485.967	.007
7	14449.909	-.010	14447.943	-.008	14485.644	-.003	14487.668	.004
8	14446.442	-.017	14444.500	-.004	14487.208	-.014	14489.253	.003
9			14440.948	.007	14488.669	-.009	14490.716	.000
10	14439.201	.006	14437.267	.006	14490.008	-.007	14492.054	-.009
11	14435.394	.006	14433.469	.004	14491.238	.005	14493.290*	-.001
12	14431.473	.007	14429.571	.018	14492.329	-.004	14494.395	-.004
13	14427.439	.012	14425.514	-.009	14493.290*	-.022	14495.365	-.023
14	14423.299*	.027	14421.391	.014	14494.170	-.002	14496.241	-.016
15	14419.012	.012	14417.130	.016	14494.900	-.012	14496.985	-.020
16	14414.640	.029	14412.739	.005	14495.520	-.011	14497.624	-.009
17	14410.102	-.004	14408.246	.009	14496.036	.007	14498.149	.010
18	14405.482	-.001	14403.622	-.001	14496.409	.003	14498.520	-.005
19	14400.781*	.038	14398.882	-.009	14496.671	.010	14498.780	-.008
20					14496.807*	.013	14498.933*	.003
21					14496.807*	.003	14498.933*	-.015

* blended lines

TABLE 4
$^{18}O_2$

	$P_{Q(N)}$		$P_{P(N)}$		$R_{R(N)}$		$R_{Q(N)}$	
N	Obs.	o.-c.	Obs.	o.-c.	Obs.	o.-c.	Obs.	o.-c.
1			14448.277	.000	14455.607	.001	14457.515	.000
3	14444.865	-.014	14442.828	.002	14459.928	.002	14461.893	.002
5	14438.930	.008	14436.922	-.003	14463.786	-.006	14465.788	.001
7	14432.550	.011	14430.581	.009	14467.204	.002	14469.218	-.002
9	14425.708	-.005	14423.760	-.009	14470.143	-.013	14472.188	-.006
11	14418.443	.004	14416.514	-.001	14472.650	-.002	14474.697*	-.012
13	14410.713	-.004	14408.806	-.006	14474.697*	.009	14476.770	.008
15	14402.559	.014	14400.655	-.002	14476.259	-.003	14478.350	-.003
17	14393.924	.001	14392.054	.003	14477.376	.004	14479.488	.008
19	14384.844	-.005	14382.975	-.019	14478.017	.001	14480.137	-.003
21	14375.339	.016	14373.526	.042	14478.190	-.002	14480.330	-.002
23	14365.328	-.016	14363.524	.003	14477.897	.001	14480.051	-.002
25	14354.891	-.020	14353.089	-.014	14477.132	.005	14479.313	.014
27	14344.012	-.009	14342.227	-.003	14475.893	.012		
29	14332.665	-.010	14330.888	-.011	14474.169	.014		
31	14320.868	-.003	14319.119	.009	14471.934	-.014		
33	14308.607	.000	14306.863	.002				
35			14294.160	.011				

* blended lines

TABLE 5
$^{17}O_2$

	$P_{Q(N)}$		$P_{P(N)}$		$R_{R(N)}$		$R_{Q(N)}$	
N	Obs.	o.-c.	Obs.	o.-c.	Obs.	o.-c.	Obs.	o.-c.
0							14490.945	.021
1			14483.824	.003	14491.583	.005	14493.462	-.009
2	14483.144	-.002	14481.009	.014	14493.917	-.005	14495.858	.004
3	14480.109	-.008	14478.072	.024	14496.148	.003	14498.103	.001
4	14477.022	.011	14474.982	.001	14498.249	.002	14500.203	-.020
5	14473.797	-.001	14471.792	-.002	14500.203	-.025	14502.212	-.007
6	14470.477	.005	14468.487	.001	14502.074	-.013	14504.090	-.001
7	14467.035	.006	14465.053	-.006	14503.816	-.009	14505.848	.007
8	14463.461	-.007	14461.513	.002	14505.436	-.004	14507.467	-.001
9	14459.795	.007	14457.851	.008	14506.942	.008	14508.963	-.010
10	14455.994	.005	14454.055	.000	14508.302	-.003	14510.342	-.012
11	14452.079	.008	14450.151	.004	14509.558	.004	14511.612	-.001
12	14448.035	.003	14446.114	-.005	14510.674	-.006	14512.744	-.004
13	14443.875	.001	14441.971	.000	14511.673	-.010	14513.751	-.009
14	14439.579	-.017	14437.694	-.008	14512.555	-.007	14514.659	.011
15	14435.192	-.006	14433.313	.000	14513.325	.008	14515.412	-.001
16	14430.692	.013	14428.802	-.001	14513.938	-.011	14516.063	.010
17	14426.035	-.005	14424.170	-.003	14514.465	.010	14516.580	.011
18	14421.270	-.010	14419.426	.004	14514.848	.011	14516.965	.006
19	14416.387	-.012	14414.552	.002	14515.104*	.010	14517.239*	.014
20	14411.377	-.021	14409.549	-.008	14515.225*	.000	14517.374*	.010
21	14406.276	.001	14404.446	.003	14515.225*	-.005	14517.374*	-.004
22	14401.040	.009	14399.219	.012	14515.104*	-.005	14517.239*	-.026
23	14395.689	.023	14393.856	.006				
24	14390.157	-.022	14388.356	-.016				
25	14384.593	.023	14382.770	-.001				
26	14378.828	-.011	14377.072	.024				
27	14372.989	.004	14371.187	-.015				
28	14367.007	-.001	14365.235	.001				

including the data of both the (1,0) and (0,0) band, a more accurate set of rotational constants for the $^{17}O_2$ ground state was derived and listed in Table 7; in this procedure the spin coupling constants were estimated from the other isotopomers (λ_0' and μ_0 scaled proportional to B and μ_0' scaled proportional to B^2) and kept fixed in the fit.

TABLE 6
Molecular Constants for the $b^1\Sigma_g^+$, $v = 1$ Excited State of Molecular Oxygen Isotopomers

	$^{16}O_2$ (a)	$^{16}O^{17}O$	$^{16}O^{18}O$	$^{18}O_2$	$^{17}O^{18}O$	$^{17}O_2$
B	1.372951 (18)	1.332761 (15)	1.29727 (3)	1.221495 (15)	1.25710 (3)	1.292776 (14)
D	5.397 (50) 10^{-6}	5.11 (2) 10^{-6}	4.80 (8) 10^{-6}	4.28 (2) 10^{-6}	4.77 (8) 10^{-6}	4.95 (2) 10^{-6}
ν_{10}	14526.9976 (12)	14507.583 (2)	14490.145 (3)	14452.164 (2)	14470.146 (3)	14487.858 (3)
Δ_{off}	-0.450	-0.4645	-0.478	-0.509	-0.494	-0.480

Note. Δ_{off} refers to the calculated offset of the $N = 0$, $J = 1$ level to the trace of the Hamiltonian, chosen as the zero energy. All values in cm^{-1}.

[a] Values for $^{16}O_2$ taken from Ref. (*8*).

TABLE 7

Molecular Constants for the $X^3\Sigma_g^-$, $v = 0$ Ground State of $^{17}O_2$ as Obtained from a Combined Fit to the *B-X* (1,0) and (0,0) Bands

B_0	1.353038 (7)
D_0	4.349 (10) x 10^{-6}
λ_0	1.9846762 [a]
λ_0'	1.8 x 10^{-6} [a]
μ_0	-7.9 x 10^{-3} [a]
μ_0'	-8.0 x 10^{-9} [a]

[a] Constants estimated from values for other isotopomers (*18, 19*).

4. CONCLUSION

Transition frequencies of the $b^1\Sigma_g^+$–$X^3\Sigma_g^-$ (1,0) band were measured for $^{16}O^{17}O$, $^{16}O^{18}O$, $^{18}O_2$, $^{17}O^{18}O$, and $^{17}O_2$ isotopomers, with an accuracy of 0.01 cm^{-1}, under pressure conditions, where pressure shifts are negligibe. Combined with previous work (*5, 8, 14*) spectral positions of the atmospheric *A* and *B* bands are now known with high accuracy for all isotopomers of oxygen.

ACKNOWLEDGMENT

The authors acknowledge support from the Space Research Organization Netherlands.

REFERENCES

1. V. D. Galkin, *Opt. Spectrosc.* **47,** 151–153 (1979).
2. L. P. Giver, R. W. Boese, and J. H. Miller, *J. Quant. Spectrosc. Radiat. Transfer* **14,** 793–802 (1974).
3. R. R. Gamache, A. Goldman, and L. S. Rothman, *J. Quant. Spectrosc. Radiat. Transfer* **59,** 495–509 (1998).
4. B. Minaev, O. Vahtras, and H. Ågren, *Chem. Phys.* **208,** 299–311 (1996).
5. H. B. Babcock and L. Herzberg, *Astrophys. J.* **108,** 167–190 (1948).
6. D. L. Albritton, W. J. Harrop, A. L. Schmeltekopf, and R. N. Zare, *J. Mol. Spectrosc.* **46,** 103–118 (1973).
7. A. J. Phillips and P. A. Hamilton, *J. Mol. Spectrosc.* **174,** 587–594 (1995).
8. A. J. Phillips, F. Peters, and P. A. Hamilton, *J. Mol. Spectrosc.* **184,** 162–166 (1997).
9. A. O'Keefe and D. A. G. Deacon, *Rev. Sci. Instr.* **59,** 2544–2551 (1988).
10. P. Zalicki and R. N. Zare, *J. Chem. Phys.* **102,** 2708–2717 (1995).
11. R. T. Jongma, M. G. H. Boogaarts, I. Holleman, and G. Meijer, *Rev. Sci. Instr.* **66,** 2821–2828 (1995).
12. J. J. Scherer, J. B. Paul, A. O'Keefe, and R. J. Saykally, *Chem. Rev.* **97,** 25–52 (1997).
13. J. T. Hodges, J. P. Looney, and R. D. van der Zee, *Appl. Opt.* **35,** 4112–4116 (1996).
14. H. Naus, A. de Lange, and W. Ubachs, *Phys. Rev.* **A56,** 4755–4763 (1997).
15. T. G. Slanger, D. L. Huestis, P. C. Cosby, H. Naus, and G. Meijer, *J. Chem. Phys.* **105,** 9393–9402 (1996).
16. S. Gerstenkorn and P. Luc, "Atlas du spectre d'absorption de la molecule de l'iode entre 14000–15600 cm^{-1}," CNRS, Paris, 1978.
17. G. Rouillé, G. Millot, R. Saint-Loup, and H. Berger, *J. Mol. Spectrosc.* **154,** 372–382 (1992).
18. W. Steinbach and W. Gordy, *Phys. Rev.* **A11,** 729–731 (1975).
19. G. Cazolli, C. Degli Esposito, P. G. Favero, and G. Severi, *Nuovo Cimento* **B62,** 243–254 (1981).